

ROBUST REGISTRATION OF CALCIUM IMAGES BY LEARNED CONTRAST SYNTHESIS

John A. Bogovic, Philipp Hanslovsky, Allan Wong, Stephan Saalfeld

HHMI Janelia Research Campus
19700 Helix Drive, Ashburn, VA 20147

ABSTRACT

Multi-modal image registration is a challenging task that is vital to fuse complementary signals for subsequent analyses. Despite much research into cost functions addressing this challenge, there exist cases in which these are ineffective. In this work, we show that (1) this is true for the registration of in-vivo *Drosophila* brain volumes visualizing genetically encoded calcium indicators to an nc82 atlas and (2) that machine learning based contrast synthesis can yield improvements. More specifically, the number of subjects for which the registration outright failed was greatly reduced (from 40% to 15%) by using a synthesized image.

Index Terms— Image Registration, Machine Learning

1. INTRODUCTION

Two photon confocal microscopy with genetically encoded calcium indicators has been used successfully for the monitoring of neural activity in defined neuronal subtypes, for instance, in the *Drosophila* antennal lobe[1]. To monitor larger, more heterogeneous populations of neurons in the whole brain, it is both necessary and challenging to identify the activated neuron reliably. Neuron identification within a large pool of references greatly benefits from registration to the reference [2]. Here, we use the fruit fly *Drosophila melanogaster* as our model organism, and experiment with different approaches to align baseline fluorescence images of experimental brains to a bridging template brain with the same driver line and a neuropil marker (see section 2.1). The neuropil marker is then used to align the template brain to a database of individually segmented neurons.

While both the template and experimental images measure similar quantities, they are imaged with different modalities and thus have differing image content, noise properties, and dynamic range. Multi-modal image registration is a common and challenging task in medical and biological imaging and an active area of research.

1.1. Related work

Kybic et al. [3] simultaneously segmented and registered histological images. The registration step minimizes the mu-

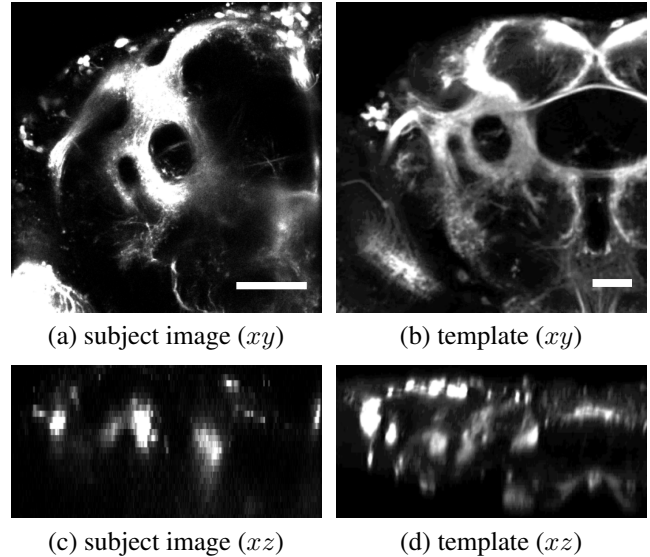


Fig. 1: Example subject (a,c) and template (b,d) image. Notice the low z -resolution in the subject (c) compared to the approximately isotropic template (d). Scale bars 50 μm .

tual information of class labels. This approach is an excellent choice when the modalities have corresponding, but differently appearing pixel classes but may have difficulties in cases where the boundaries of various labels are unclear, or when image content differs significantly.

A different approach appears in Roy et al. [4] where the target modality is “synthesized” from the source modality directly. Their proposed method uses a registered pair (one from each modality) of images of the same subject as an “atlas.” Their method uses a patch-based search with heuristics designed for MRI to estimate the target modality from source. They show that intra-modality registration using the result outperforms inter-modality methods.

In their survey, Sotiras et al. [5] describe many other alternative approaches. Most related to our method are the approaches by Wein et al. [6] who simulate an ultrasound image from CT using imaging physics and known tissue properties, and Michel et al. [7] who use a mixture of experts and MRF to learn the probability of a target intensity conditioned on a source image patch.

2. METHODS

Our method is inspired by other inter-modality registration methods that “synthesize” a target image modality from a source image modality. Unlike much previous work, an “atlas pair” of images (one from each modality) is not available for our application. Instead, we manually register the two modalities for some set of subjects to create a “silver standard atlas.” Given the inherent error in this atlas, we opt to learn a mapping between the modalities via a classifier, similar to [7], rather than use patch correspondences directly, as in [4]. Once this mapping is learned, it can be applied to the subject modality to produce an image more similar to the target, with the hope that the resulting image can be more reliably registered with standard algorithms than the original modality.

2.1. Imaging and Preprocessing

We express the calcium indicator GCaMP6s in Fruitless neurons and collect volumetric images at $512 \times 512 \times 42$ pixels (at $0.43 \times 0.43 \times 5 \mu\text{m}/\text{pixel}$ resolution). Each volume was collected at 0.95 Hz and 200 volumes were averaged to create a baseline volume image with high signal to noise. This serves as the subject image. The 4D volumes can be analyzed independently to extract calcium signals.

Separately, we collected the bridging template brain of the same Fruitless driver line crossed with *myr::GFP*, which uniformly labels the membrane of the neuron. The brain was then immunohistochemically stained with anti-GFP and with nc82 antibodies to label the neuropils, cleared with DPX and imaged with a Zeiss confocal using a 20 \times air objective. The nc82 channel was then used to register the *Fru-myr::GFP* sample to a common reference. This bridging template brain, after warping to the common reference, has $1 \times 1 \times 1 \mu\text{m}/\text{pixel}$ resolution.

We preprocess the images by clipping intensities above the 99th percentile, followed by Gaussian smoothing with a $1.5 \times 1.5 \times 1.5 \mu\text{m}$ kernel, and finally linearly scaling the intensities to the range [0, 255]. This was applied to both the template and subject images.

2.2. Baseline Registration

We attempt to register the subject images to the template using the SyN algorithm [8] (part of the ANTs¹ toolbox) using several cost functions: sum of squared differences (SSD), normalized cross correlation (CC), and mutual information (MI). The preprocessed template and subject images were used as inputs to SyN.

2.3. Ground Truth

We first manually coregistered several subject image volumes to the template by placing corresponding landmarks and using

¹<http://stnava.github.io/ANTs>

a thin plate spline transformation to generate a dense warping. This was important because a set of registered images is needed in order to learn a mapping between the modalities, as will be explained below in section 2.4.

The registration task is quite challenging even for human annotators. One human annotator (JB) placed landmarks on all images to produce a registration. Another annotator (SS) began with the first annotator’s landmarks on the target images only, and independently placed landmarks on the moving image. Using these measurements, we can determine whether a given registration algorithm performs the task with “human-like” precision.

To facilitate manual registration with landmark placement, we developed *BigWarp*², a tool for fast, interactive, and deformable alignment of large 2D and 3D images. It builds upon *BigDataViewer* [9] for visualization and data sources which enables rapid navigation of very large images with arbitrary 3D reslicing and zoom. We made *BigWarp* publicly available through the ImageJ distribution Fiji [10]³ contributing real time deformable 2D and 3D transformation for almost arbitrarily large images.

2.4. Learning the synthesis mapping

We used manually registered subject + template image pairs to learn a mapping (“synthesis”) from the subject intensities to the template intensities. This analysis was done in subject image space in order to avoid the significant upsampling that would be necessary to transform the lower-resolution subject image into the template image space.

To learn the mapping from source to target modalities, we used boosted decision trees (BDT) [11] and a random forest (RF) classifier (using the implementation in VIGRA [12]).

Boosted decision trees were trained using a squared loss for 10k iterations, with a shrinkage factor of 0.01, a subsampling factor of 0.2, to a max depth of 3. The random forests were trained to purity with 1000 trees and a subsampling factor of 0.1. We ran experiments using two kinds of features for both algorithms: (a) pixel intensities inside a $5 \times 5 \times 3$ patch around the pixel of interest, (b) multi-scale gradient, intensity, and texture based features. For both methods, 200k samples were randomly drawn from two training subjects. Surprisingly, the resulting registrations using (b) had larger errors across all subjects compared to using (a). The classifier does not predict the continuous pixel intensity of the template image, but one of 10 classes derived from binning the pixel intensities by every 10th percentile. We experimented with other schemes as well; this had the best performance of those we tried.

Once a classifier is learned, we apply it to all pixels of the subject image to obtain the “synthetic” template image. This

²<https://github.com/saalfeldlab/bigwarp>

³<https://fiji.sc/bigwarp>

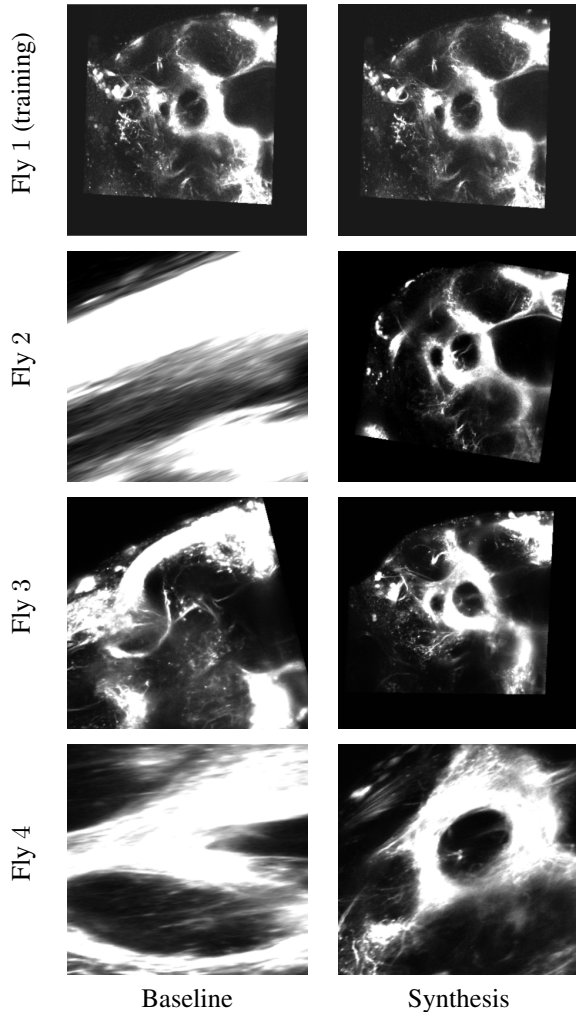


Fig. 2: Registration results for baseline (left) and random forest synthesis (right). Both methods succeed for fly 1 (one of the training subjects), only the synthesis succeeds for flies 2 and 3, and both methods fail for fly 4.

is registered with SyN, with identical parameters as used for the baseline registration (see section 2.2).

3. EXPERIMENTS

We inspected each registration result using CC visually and 4 of 7 baseline results are (qualitatively) useful, where 6 of 7 synthesis results are useful. F shows four of these results for baseline (left) and synthesized (RF) experiments for three different subjects, all using ANTS with a cross correlation cost.

We computed errors (euclidean distance) between landmarks placed by a human annotator, and landmarks transformed by a registration. Fig. 2 shows landmark errors for various experimental images and registration techniques. The

left group of plots shows errors for the two subjects used to train the contrast synthesis mapping; the right group shows errors for the four subjects left out for testing. The leftmost scatter group (black) plots the inter-human landmark placement error. The next nine plots show errors for the “baseline” registration method (the SyN algorithm on smoothed image data), and the proposed synthesis approach for two different classifiers, each with three choices of cost function. We note that for some subjects, the SSD cost resulted in a transformation with a singular affine part which is equivalent to total failure. We indicated those by a red x -axis label.

The pattern shown by example in Fig. 2 is consistent with and explains the distribution of errors in Fig. 3. Many errors are small (on the order of inter-human error). Catastrophic landmark transfer errors are more common in the baseline than in any of the synthesized images.

4. DISCUSSION

A surprising outcome of our experiments is the extent to which mutual information underperformed relative to cross correlation for both baseline and synthesis experiments. This could be due to the rather small dynamic range of the acquired images. We also observed that the warp field estimated by SyN was often very small for subjects that failed. This seemed to follow a poor initial estimate of the affine part of the transformation which may explain why an additional warp could not further reduce the cost function.

Another observation of note is the fact that our method was trained only on subjects for which the baseline method succeeded. Still, when applied to more challenging subjects (for which the baseline failed) the classifier generalized sufficiently well to produce a synthesized image that could be registered successfully to the template. Training on larger and more diverse set of subjects could further improve robustness in the future.

We also note that unlike [4], our proposed method does not use heuristics to aid in the synthesis mapping. As such, we hope that this approach may be applicable to a wider variety of domains. However, a drawback is the fact that the synthesized images produced here do not resemble the target modality to a human (but evidently are more similar to cost functions used in registration). Exploring alternative models or algorithms to implement the mapping (convolutional networks, or mixture of experts, as in [7]) are interesting avenues of future research.

In conclusion, our results show that learning to synthesize the template modality from the subject modality results in more robust registration performance (i.e. fewer subject registrations resulted in unusable results). Secondly, cross correlation outperforms other cost function for the registration of these image data.

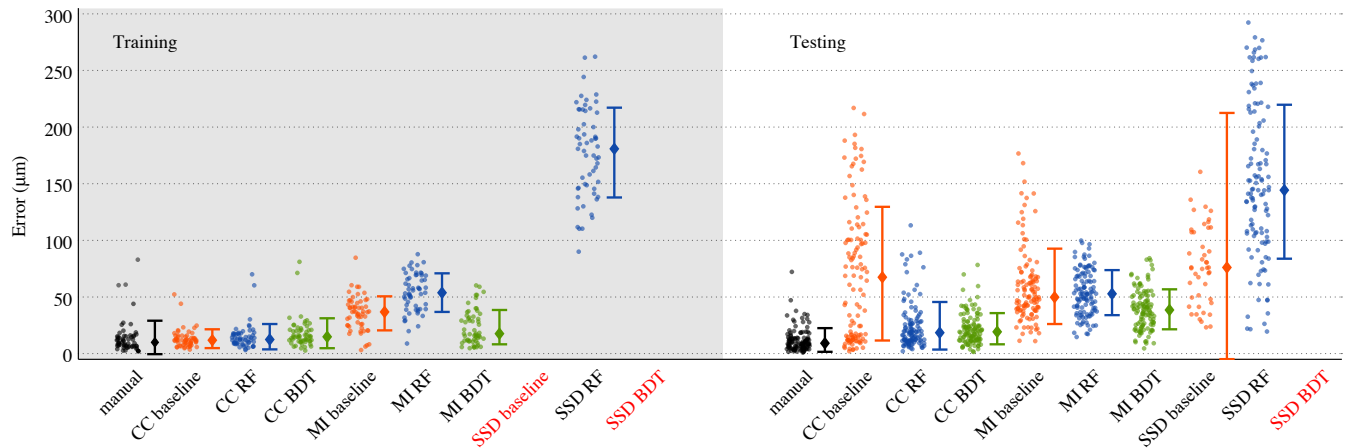


Fig. 3: A scatter plot showing landmark errors for different registration methods for training (left group) and testing subjects. In each group, the left most points (black) show inter-human landmark error. Next are baseline (orange), random forest (RF) (blue), and boosted decision tree (BDT) (green). Results for each of these three methods is given with three cost functions in ANTS, cross correlation (CC), mutual information (MI), and sum of squared differences (SSD). The landmark errors are plotted as points, the median as a diamond, and the bar gives the mean \pm one standard deviation. There are 72 and 180 landmarks for the training and testing subjects, respectively.

5. ACKNOWLEDGMENTS

The authors would like to thank Barry Dickson and Kaiyu Wong for their valuable feedback and discussions regarding image acquisition.

References

- [1] J. W. Wang, A. M. Wong, J. Flores, L. B. Vosshall, and R. Axel, “Two-photon calcium imaging reveals an odor-evoked map of activity in the fly brain,” *Cell*, vol. 112, no. 2, pp. 271–82, 2003.
- [2] M. Costa, J. D. Manton, A. D. Ostrovsky, S. Prohaska, and G. S. Jefferis, “Nblast: Rapid, sensitive comparison of neuronal structure and construction of neuron family databases,” *bioRxiv*, 2015.
- [3] J. Kybic and J. Borovec, “Automatic simultaneous segmentation and fast registration of histological images,” in *Int. Symp. Biomed. Imag.*, 2014, pp. 774–777.
- [4] S. Roy, A. Carass, and J. L. Prince, “Magnetic Resonance Image Example-Based Contrast Synthesis,” vol. 32, no. 12, pp. 2348–2363, 2013.
- [5] A. Sotiras, C. Davatzikos, and N. Paragios, “Deformable medical image registration: a survey,” *IEEE Trans Med Imaging*, vol. 32, no. 7, pp. 1153–1190, 2013.
- [6] W. Wein, S. Brunke, A. Khamene, M. R. Callstrom, and N. Navab, “Automatic CT-ultrasound registration for diagnostic imaging and image-guided intervention,” *Medical Image Analysis*, vol. 12, no. 5, pp. 577–585, 2008.
- [7] F. Michel and N. Paragios, “Image transport regression using mixture of experts and discrete markov random fields,” in *Int. Symp. Biomed. Imag.*, 2010, pp. 1229–1232.
- [8] B. B. Avants, C. L. Epstein, M. Grossman, and J. C. Gee, “Symmetric Diffeomorphic Image Registration with Cross-Correlation: Evaluating Automated Labeling of Elderly and Neurodegenerative Brain,” *Med Image Anal*, vol. 12, no. 1, pp. 26–41, 2009.
- [9] T. Pietzsch, S. Saalfeld, S. Preibisch, and P. Tomancak, “Big-DataViewer: visualization and processing for large image data sets,” *Nature Methods*, vol. 12, no. 6, pp. 481–483, may 2015.
- [10] J. Schindelin, I. Arganda-Carreras, E. Frise, et al., “Fiji: an open-source platform for biological-image analysis,” *Nature methods*, vol. 9, no. 7, pp. 676–82, jul 2012.
- [11] C. Becker, R. Rigamonti, V. Lepetit, and P. Fua, “Supervised feature learning for curvilinear structure segmentation,” in *MICCAI*, 2013, vol. 8149 LNCS, pp. 526–533.
- [12] U. Köthe, “Reusable Software in Computer Vision,” in *Handbook on Computer Vision and Applications*, P. G. B. Jähne, H. Haußecker, Ed. 1999, vol. 3, Academic Press.